To be published in American Physical Society Physical Review B journal and on nepp.nasa.gov.

Time-Dependent Insulation Resistance Degradation in Multilayer Ceramic Capacitors with Base-Metal Electrodes

Donhang (David) Liu

ASRC Federal Space and Defense, Inc.
7515 Mission Drive, Suite 200, Seabrook, MD 20706

Work performed for NASA Goddard Space Flight Center
8800 Greenbelt Road, Greenbelt, Maryland, 20771, USA

Insulation resistance degradation in Ni-$BaTiO_3$ multilayer ceramic capacitors has been characterized by the measurement of time to failure and DC leakage current as a function of stress time under highly accelerated life stress test conditions. The leakage current-time dependence follows an exponential law, and a characteristic growth time τ_{SD} can be determined. A greater value of τ_{SD} represents a slower IR degradation process. Oxygen vacancy migration and localization at the grain boundary region has resulted in the reduction of the Schottky barrier height and has been found to be the main reason for IR degradation in Ni-$BaTiO_3$ capacitors. The reduction of barrier height as a function of time follows an exponential relation of $\phi(t) = \phi(0)\mathrm{e}^{-2\mathrm{Kt}}$, where degradation rate constant $K = K_0 e^{-\frac{E_k}{kT}}$ is inverse to the mean time to failure (MTTF) and can be simply determined using an Arrhenius plot. For oxygen vacancy electromigration, a lower barrier height $\phi(0)$ will favor a slow IR degradation process, but a lower $\phi(0)$ will also promote electronic conduction and will accelerate IR degradation. As a result, a moderate barrier height $\phi(0)$ (and therefore a moderate IR value) with a longer MTTF (smaller degradation rate constant K) will result in a minimized IR degradation process and the most improved reliability in Ni-$BaTiO_3$ multilayer ceramic capacitors.

I. INTRODUCTION

Time-dependent degradation in insulation resistance (IR) related to oxygen vacancy migration has been considered to be the primary cause of reliability degradation of multilayer ceramic capacitors (MLCCs) with base-metal electrodes (BME). The behavior is characterized by a slow increase in the leakage current under an applied direct-current (DC) field stress. In order to reveal IR degradation in a time-efficient manner, MLCCs are often degraded under highly accelerated life stress testing conditions (HALST) with different temperatures and applied voltages. Previous investigation of the IR degradation has shown that the degradation may be caused by three possible

factors for $BaTiO_3$-based BME MLCCs: the dielectric layer, the $BaTiO_3$ grain boundaries, and the Ni-$BaTiO_3$ internal electrode interfaces. [1-4]

Unlike traditional $BaTiO_3$-based MLCCs with precious-metal electrodes (PMEs), BME MLCCs are co-fired in a reducing atmosphere to avoid oxidation of the electrodes. Despite the reoxidation process, there are still a large number of oxygen vacancies that are accommodated in the $BaTiO_3$ dielectric layers. The failure mechanism of BME MLCCs is thought to be dominated by electromigration of oxygen vacancies through the grain boundaries in the dielectric layers.[5–8] Waser et al. [9-12] studied the IR degradation in ambient-fired $SrTiO_3$ ceramic and acceptor-doped single crystal $SrTiO_3$. The results showed that IR degradation begins with oxygen vacancy electromigration toward the cathode with respect to time, field, and temperature. Segregation of defects and dopants is found at the grain boundaries during the sintering process and results in the formation of space charge layers at the grain boundaries. The formation of double Schottky depletion layers at the grain boundaries of ceramic $BaTiO_3$ and their impact on the properties of $BaTiO_3$ ceramics was first proposed by Heywang[13] in order to explain the unique positive temperature coefficient of resistance (PTCR) behavior around the Curie temperature, which only existed in the donor-doped semiconducting $BaTiO_3$ ceramics. Based on this model, the depletion barriers are formed because of the electron trapping by acceptor states at grain boundaries. Jonker[14-15] later extended the Heywang model, considering the influence of ferroelectric polarization on resistivity below the Curie temperature. In $BaTiO_3$-based MLCCs, the depletion layers are believed not only to be depleted of electron carriers and therefore to be highly resistive, but also to act as electrical barriers against oxygen vacancy electromigration and thus to slow down the degradation process.[2, 10, 16-17] Although both high resistance depletion layers at grain boundaries and at electrode interfaces limit the electrical conduction of electrons and the transport of oxygen vacancies across dielectric layers, oxygen vacancy migration is blocked by electrode interfaces, and a majority of oxygen vacancies are trapped at the electrode interface region and are neutralized by the reduction of Ti^{4+} near the cathode. This agrees with a later-published work about the computational analysis of local atomic configuration and energy at grain boundaries as a result of the coordination numbers of Ti^{4+} in the region.[18]

In this paper, the IR degradation in Ni-$BaTiO_3$ MLCCs was investigated for two commercial BME capacitors with different reliability levels from the same manufacturer. The capacitors are forced

to degrade under HALST conditions at different temperatures and applied voltages. The leakage currents of the capacitors are monitored and recorded as a function of the stress time until the capacitors failed electrically. The time-dependence of the leakage current has been found to fit well to an exponential relationship. A time-dependent Schottky barrier layer model has been developed with respect to oxygen vacancy migration and localization at grain boundaries. A temperature-dependent degradation rate constant has been used to describe the IR degradation in BME MLCCs. The constant is simply an inverse to the MTTF and can be determined in a simple Arrhenius plot.

II. EXPERIMENTAL PROCEDURE

Two commercial Ni-$BaTiO_3$ MLCCs from the same manufacturer were used for this investigation. One of them (BME A) is an automotive-grade MLCC device that was qualified per AEC-Q200, a specification that was developed by the Automotive Electronics Council for passive components to be used in the harsh automotive environment. The other capacitor (BME B) is a commercial off-the-shelf product with thin dielectric layers and a high number of dielectric layers designed for high volumetric efficiency applications. Prior to electrical characterization, both capacitors were processed for construction and microstructural characterizations. Results are summarized in Table I.

Table I. Construction and Microstructural Information of the Ni-$BaTiO_3$ MLCCs Used in This Investigation

Capacitor ID	Specifications	No. of Dielectric Layers	Dielectric Thickness (μm)	Avg. Grain Size (μm)	No. of Dielectric Layers per Grain
BME A	0.47uF, 50V, 0805	98	6.39	0.377	16.95
BME B	4.7uF, 16V, 0805	261	2.49	0.230	10.83

A 20-position printed circuit board (PCB) testing card was used for the characterization of BME capacitors throughout this study. All capacitors were convention solder-reflow attached on the testing card prior to testing. The soldering reflow condition complied with MIL-PRF-55681. No-clean solder paste with RMA (rosin mildly activated) flux was used. Only one reflow cycle was applied. After assembly, all capacitors were subject to an electrical test for capacitance, dielectric loss at 1 kHz, to make sure all units on the board were electrically normal.

The leakage current as a function of stress time was monitored in-situ and recorded every 1-3 seconds for each capacitor until the leakage current reached the failure criterion of 100 μA, used for all stress levels in this study. A series resistor was connected to each capacitor being tested, for the purposes of current limiting and the reading of the leakage current.

III. RESULTS AND DISCUSSION

A. Characterization of time-dependent leakage current

(1) Failure criterion of degradation

When IR degradation is accelerated under HALST conditions, a certain value of IR or a value of leakage current must be used as the failure criterion at which the time to failure (TTF) can be determined. Per MIL-PRF-123, the $BaTiO_3$-based MLCCs for high-reliability applications were built with a minimum dielectric thickness of 25 μm when the rated voltage is over 50V. In this case, the leakage current level was very low, even under HALST conditions. The MLCC was considered a failure when IR at a given stress condition degraded three to four orders below its initial value.[19-20] Waser et al. have also defined characteristic lifetime t_{ch} at which the leakage current has risen one decade above its minimum value to evaluate the degradation rate.[10] With the progress in Ni-$BaTiO_3$ MLCC development, the dielectric thickness was reduced significantly, even below one micron. As a result, the leakage current has increased significantly, and Ni-$BaTiO_3$ MLCCs are considered to have failed at a fairly low IR value. Some reports define the TTF as the time at which IR is degraded to a value of 500 kΩ,[21-22] 1,000 kΩ,[23] or 90% of its initial value[4] , while others set a constant leakage current limit at 100 μA for all of the stress conditions being used.[24-28] After reviewing most of the failure criteria that have been used for determining the TTF of $BaTiO_3$ MLCCs, this study uses a single current limit of 100 μA to determine the TTF for all stress levels and for all MLCC samples, based on the following considerations:

During the accelerated life testing, each MLCC was connected in series to a current-limiting resistor with a DC power supply. The voltage drop across the series resistor was measured and used to calculate the leakage current of the capacitor. MLCCs with greater dielectric thicknesses usually require a higher applied voltage to generate enough failures within a reasonable period of stress time, and the 100 μA limit will result in a higher IR value at a given TTF. On the other hand, MLCCs with thinner dielectric layers often require a lower applied voltage for degradation

and result in a lower IR value for a failure. Since the voltage drop on the current-limiting resistor depends on the current value, a leakage current higher than 100 μA can result in a voltage drop on the current-limiting resistor of more than 5% of the overall applied voltage. Although this voltage drop can be reduced if a smaller-value resistor is used, the voltage value reading on a small resistor may be too low to ensure the accuracy of the IR measurement. For example, when an MLCC with a 100 kΩ resistor was accelerated at 150V, the voltage drop will be 100 kΩ·100μA = 10V, which is 6.7% of the total applied voltage. For a 1 kΩ resistor, the voltage drop is only 0.1V across the resistor, which may be too low to show the details of the leakage changing with the stress time. In this study, the values of the resistor are chosen such that the maximum voltage drop at the resistor will be no more than 3% of the applied voltage under all stress conditions.

(2) Characteristics of leakage current

FIG. 1 shows measured leakage current data as a function of applied voltage and temperature for BME A and BME B. All capacitors had a near-linear increase with time to a certain point, and then some of them failed with a catastrophic failure process, characterized by a time-accelerating increase in leakage current; others, however, maintained the near-linear increase until 100 μA was reached. Further details about the characterization of the failure patterns and the method to determine the acceleration factors have been discussed previously.[28]

Although the leakage data shown in FIG. 1 appear to be linear for most of the stress time measured, the curve-fitting results have shown that the exponential form of

$$I = I(t_0)e^{\left(\frac{t-t_0}{\tau_{SD}}\right)}, \quad (1)$$

actually fits most of the leakage data better than a linear form. In Eq. (1), I is the measured leakage current, $I(t_0)$ is the leakage value at $t=t_0$, and τ_{SD} is a characteristic exponential growth time.

FIG. 2 shows curve-fitting results using Eq. (1) for two capacitor samples with different failure patterns. The C13 with a near-linear increase in leakage fits very well to Eq. (1). Although C7 shows a catastrophic failure characterized by a rapid leakage current increase, the majority of the leakage data still fit well to Eq. (1), and a comparable τ_{SD} to C13 is obtained.

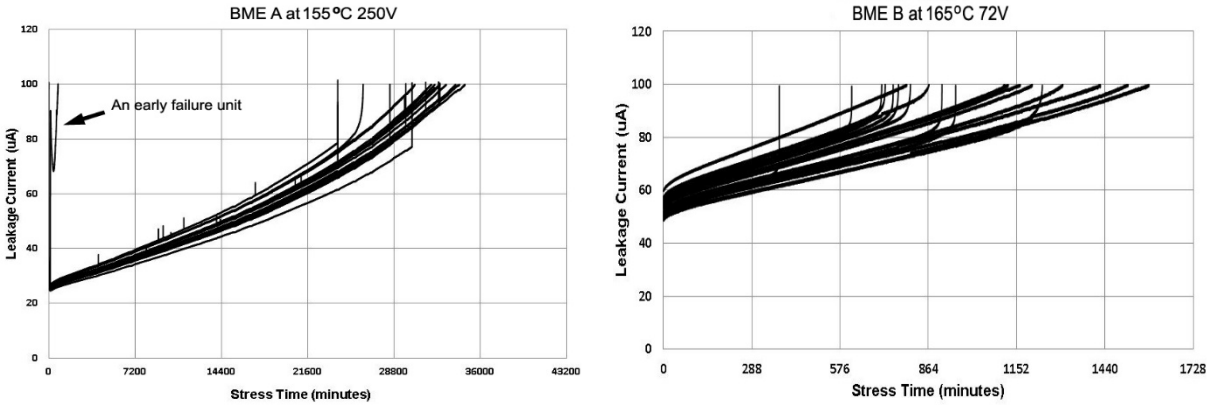

FIG. 1. Measured leakage current as a function of stress time for BME A (right), tested at 155°C and 250V (5.0x rated voltage); and for BME B (left), tested at 165°C and 72V (4.5x rated voltage). One early failure unit was found for the BME A group. The arrow indicates an early failure unit.

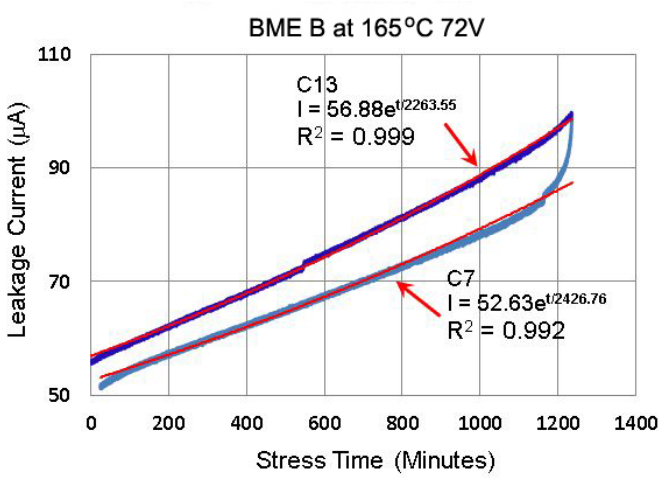

FIG. 2. Examples of curve-fitting using Eq. (1) for two BME B capacitor samples with different failure patterns. Both appear to fit well to the exponential form of Eq. (1).

In general, a larger value of τ_{SD} indicates a slower degradation process. The meaning of τ_{SD} can be illustrated by the following example:

Let I_1 and I_2 be the leakages at t_1 and t_2, respectively, for a slow degradation failure. If one assumes $\frac{I_2}{I_1} = 2$, then Eq. (1) can be rewritten as:

$$\frac{I_2}{I_1} = e^{\left(\frac{t_2 - t_1}{\tau_{SD}}\right)} = e^{\left(\frac{\Delta t}{\tau_{SD}}\right)} = 2,$$

and

$$\tau_{SD} = \frac{\Delta t}{ln(2)} \approx 1.4427 \cdot \Delta t, \quad (2)$$

where Δt is the time at which the leakage current doubles its value. The greater the value of τ_{SD}, the longer the time span of a degradation failure.

(3) Determination of average τ_{SD}($\langle\tau_{SD}\rangle$) and MTTF

To repeat the curve-fitting step using Eq. (1) and to record the TTF at 100 μA, all TTF and τ_{SD} data can be determined. Table II summarizes the TTF and τ_{SD} data for BME B at 165°C and 72V. When the leakage current of each MLCC is recorded during the accelerated IR degradation, the TTF and parameter τ_{SD} that characterizes the IR degradation rate can both be obtained at a given stress level.

Table II. TTF and τ_{SD} Determined from FIG. 1 for BME B at 165°C and 72V

Cap ID on testing board	TTF (min)	τ_{SD} (min)
C15	377.26	1741.10
C12	614.70	1789.10
C16	712.00	1705.20
C19	723.40	1832.80
C14	749.30	1849.21
C10	766.34	1881.41
C18	793.25	1803.03
C4	805.29	1935.94
C17	866.30	1866.25
C3	908.27	2278.60
C9	953.18	2204.88
C2	1112.39	2158.85
C8	1124.51	2104.98
C6	1163.47	2149.60
C0	1203.19	2216.00
C7	1235.54	2426.76
C13	1302.47	2263.55
C11	1425.38	2410.67
C1	1515.23	2574.77
C5	1583.30	2506.14

τ_{SD} has been found to decrease with decreasing TTF, but at a much slower rate, indicating that for the majority of the time, the capacitors have a similar degradation rate. It has also been noticed that τ_{SD} is always longer than TTF. This is true for all of the BME MLCCs from this manufacturer that have been investigated.

The MTTF can be determined from the Weibull plot of TTF data shown in Table II as:

$$MTTF = \eta\Gamma(1 + \beta^{-1}), \tag{3}$$

where slope β is the dimensionless shape parameter whose value is often characteristic of the particular failure mode, η is the scale parameter that represents the point at which 63.2% of the population has failed, and $\Gamma(x)$ is the gamma function of x. (Note, for example, that $\Gamma(1+1/\beta)$ ranges from 0.887 to 0.900 as β ranges from 2.5 to 3.5.)

The scale parameter η from the Weibull plot of all τ_{SD} data shown in Table II is designated to the average value of $\langle\tau_{SD}\rangle$. For BME B at 165ºC and 72V, the following values were obtained: MTTF = 998.04 minutes and $\langle\tau_{SD}\rangle$ = 2189.61 minutes, respectively. The MTTF and $\langle\tau_{SD}\rangle$ of all MLCC samples under various stress conditions can be obtained as well if the procedure described above is repeated.

B. Time-dependent depletion layer height $\boldsymbol{\phi(t)}$

Although the formation of a double Schottky barrier layer at a grain boundary as shown in FIG. 3 was initially proposed to explain the PTCR effect in donor-doped semiconducting $BaTiO_3$ ceramics[13-15], the same barrier depletion layer model has also been suggested to explain the IR degradation in Ni-$BaTiO_3$ MLCCs [2, 4]. The typical barrier height can be expressed as

$$\phi = \frac{e^2 N_d d^2}{2\varepsilon_0 \varepsilon_r},$$

where N_d is the donor concentration, d is the depletion layer thickness, e is the electron charge, and $\varepsilon_0\varepsilon_r$ is the dielectric constant. The electro-neutrality condition in the depletion layer satisfies the following condition:[13]

$$d = \frac{n_s}{2N_d}, \tag{4}$$

where n_s is the concentration of *trapped electrons* at grain boundary acceptor states (cm^{-2}). The ϕ can be re-written as

$$\phi = \frac{e^2 n_s^2}{8\varepsilon_0 \varepsilon_r N_d}. \quad (5)$$

Above the Curie temperature, the dielectric constant obeys the Curie-Weiss law,

$$\varepsilon_r = \mathrm{C}/(T - \theta), \quad (6)$$

where $\theta = 380K$ and $C \approx 1.2\times10^5$ is the Curie-Weiss constant.[14, 29] Combining Eqs. (5) and (6) gives rise to

$$\phi = \frac{e^2 n_s^2}{8\varepsilon_0 \varepsilon_r N_d} = \frac{e^2 n_s^2 (T - \theta)}{8\varepsilon_0 C \cdot N_d}. \quad (7)$$

Eq. (7) has been often used to estimate the grain boundary barrier height in semiconducting $BaTiO_3$ ceramics.[34, 38] In Ni-$BaTiO_3$ MLCCs, N_d is mainly determined by the bulk concentration of ionized oxygen vacancies. Although oxygen vacancies migrate under an applied DC field and the weakly bonded electrons can be trapped by the surface acceptor states, the value of d in Eq. (3) is often in the submicron range, indicating that $N_d >> n_s$. Therefore, one can assume that $N_d(t) \approx N_d(0)$, and is independent on time. Therefore,

$$\frac{d\phi(t)}{dt} = \frac{d}{dt}\left(\frac{e^2 n_s^2}{8\varepsilon_0 \varepsilon_r N_d}\right) = \frac{e^2}{4\varepsilon_0 \varepsilon_r N_d}\frac{dn_s(t)}{dt}.$$

In order to determine $\frac{dn_s(t)}{dt}$ the following facts were considered: 1) $n_s(t)$ is trapped electrons at surface acceptor states in the grain boundary regions. The negative space charge due to trapped electrons is compensated by the formation of a positive space charge region near the grain boundary, which behaves like a depletion barrier layer to electron conduction. 2) The computational analysis on the trapping of oxygen vacancies at grain boundaries with respect to local atomic configuration and energy shows that grain boundaries attract oxygen vacancies and trap them at specific sites at which local cation density is lower than in the grain interior.[30]

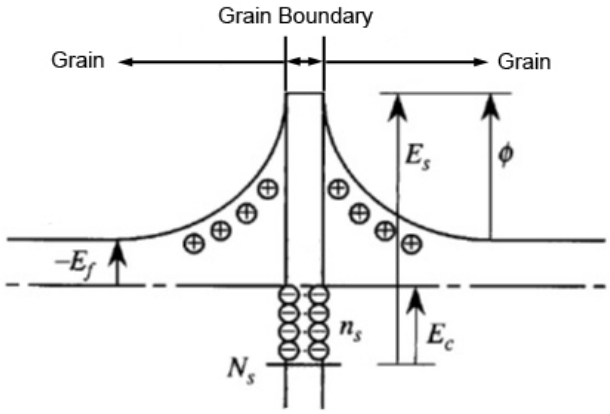

FIG. 3. Schematic illustration of the formation of a double Schottky barrier around the grain boundary of a $BaTiO_3$ ceramic capacitor.

3) Since oxygen vacancies behave like donors, they possess positive space charges when ionized. The same positive space charge in a barrier layer at a grain boundary will thus act as a resistance for positively charged oxygen vacancy diffusion in a polycrystalline $BaTiO_3$ dielectric. As a result, when an ionized oxygen vacancy migrates under a DC field and reaches the barrier layer, it has a tendency to become trapped there. The electro-neutrality condition requires that the weakly bonded two electrons that are moving in a conduction band now have to be localized in order to make the trapped oxygen vacancy neutralize and to become part of the crystalline structure. When Kroger and Vink symbols are used[31], the process can be simply described by

$$V_O^{\bullet\bullet} = V_O + 2e'. \tag{8}$$

As previously reported, the localized electrons that compensate the $V_O^{\bullet\bullet}$ localization can be trapped with the reduction of *Ti* ions surrounding the $V_O^{\bullet\bullet}$ as $Ti^{4+} + e' \rightarrow Ti^{3+}$, and $Ti^{3+} + e' \rightarrow Ti^{2+}$.[4] The reduction of Ti^{4+} will now reduce the positive space charge in the positively charged depletion layer and reduce the barrier height. Since the barrier height is balanced by the trapped electrons in surface acceptor states $n_s(t)$, the reduction in barrier height will lower the Fermi level at grain boundary and then will reduce the $n_s(t)$. However, with a further increase of localized electrons as more $V_O^{\bullet\bullet}$ are trapped and neutralized, the electrical negative feature of $n_s(t)$ will further retard the localization of electrons and reduce the localization rate of $V_O^{\bullet\bullet}$.

If we assume Δn_O is the electron concentration that has been localized to make the trapped $V_O^{\bullet\bullet}$ neutral, Δn_O should meet the following conditions: at $t = 0$, $\Delta n_O(0) = 0$, and at $t \to \infty$, $\Delta n_O = n_s(0)$, i.e., all trapped electrons at $t = 0$ in the surface acceptor states $n_s(0)$ will eventually be fully compensated by the localized electrons that neutralize the trapped $V_O^{\bullet\bullet}$. However, with a further increase of Δn_O as more $V_O^{\bullet\bullet}$ are trapped and neutralized, the electrically negative feature of $n_s(t)$ will further retard the localization of electrons and reduce the localization rate of Δn_O. Therefore, the change of Δn_O as a function of *t* can be expressed by a first-order reaction according to the reaction rate theory[32]

$$\frac{d\Delta n_O(t)}{dt} = K(t)[n_s(0) - \Delta n_O(t)],$$

and

$$\int_{\Delta n_O(0)}^{\Delta n_O(t)} \frac{d\Delta n_O(t)}{\Delta n_O(t) - n_s(0)} = \int_0^t -K(t)dt \tag{9}$$

where *K(t)* is the degradation rate constant and $n_s(0) - \Delta n_O(t) = n_s(t)$ is the trapped electron concentration at surface acceptor states at time *t*. If $\Delta n_O(t)$ is only balanced by $n_s(t)$ near the Fermi level, $K(t) = K = K_0 e^{-\frac{E_k}{kT}}$ can be simplified as a time-dependent constant in which E_k is the activation energy that is required for $V_O^{\bullet\bullet}$ to electromigrate and to be neutralized at a grain boundary region per Eq. (8) and *k* is the Boltzmann constant. Since $\Delta n_O(0) = 0$, Eq. (9) finally yields

$$\frac{n_s(0) - \Delta n_O(t)}{n_s(0)} = e^{-\mathrm{K}t},$$

and

$$\Delta n_O(t) = n_s(0)(1 - e^{-\mathrm{K}t}), \tag{10}$$

the remaining trapped electrons in acceptor states can be simply expressed according Eq. (10) as

$$n_s(0) - \Delta n_O(t) = n_s(0) - n_s(0)(1 - e^{-\mathrm{K}t}) = n_s(0)e^{-\mathrm{K}t}.$$

Combining Eqs. (5) and (10) yields a time-dependent barrier height

$$\phi(t) = \frac{e^2[n_s(0) - \Delta n_O(t)]^2}{8\varepsilon_0\varepsilon_r N_d} = \phi(0)\mathrm{e}^{-2\mathrm{Kt}}. \quad (11)$$

This relation indicates that the barrier height will exponentially decrease with time due to the oxygen vacancy migration and localization at grain boundaries.

C. Determination of degradation rate constant *K*

The measurement of *I-V* characteristics of ceramic $BaTiO_3$ inside the grain interior and at the grain boundary has shown that under an applied field of 100 kV/cm, the current density inside the grain and at the grain boundary can differ by several orders of magnitude. The difference increases significantly as temperature increases.[33] It is the grain boundary that holds the high resistivity of the ceramic $BaTiO_3$. If all grain boundaries inside a dielectric layer are assumed to have a uniform barrier height $\phi(t)$, the time-dependent resistivity $\rho(t)$ of an MLCC can be simply written as

$$\rho(t) = \rho_0 e^{\left(\frac{\phi(t)}{kT}\right)}, \quad (12)$$

where ρ_0 is the resistivity of the grain. According to Eq. (1), the time-dependent current density of an MLCC $j(t)$ is

$$j(t) = j(t_0)e^{\left(\frac{t-t_0}{\tau_{SD}}\right)} = \frac{E}{\rho(t)},$$

or

$$\rho(t) = \frac{E}{j(t_0)} e^{-\left(\frac{t-t_0}{\tau_{SD}}\right)}, \quad (13)$$

where $j(t_0)$ is the current density at $t = t_0$ and E is the applied field. Combining Eqs. (12) and (13) results in

$$\rho(t) = \rho_0 exp\left(\frac{\phi(t)}{kT}\right) = \rho_0 exp\left(\frac{\phi(0)\mathrm{e}^{-2\mathrm{Kt}}}{kT}\right) = \frac{E}{j(0)} exp\left(-\frac{t-t_0}{\tau_{SD}}\right),$$

at a given stress level, E is a constant, so that

$$\frac{t-t_0}{\tau_{SD}} \approx -\frac{\phi(0)}{kT}\mathrm{e}^{-2\mathrm{Kt}}. \quad (14)$$

Using $\langle\tau_{SD}\rangle$, the average of τ_{SD}, to replace τ_{SD}, and $e^{-x} \approx 1 - x$ when x is small, the integration of Eq. (14) results in

$$\int_0^{MTTF} \frac{t-t_0}{\langle \tau_{SD} \rangle} dt = -\int_0^{MTTF} \frac{\phi(0)}{kT} \cdot \mathrm{e}^{-2\mathrm{Kt}} dt \approx -\int_0^{MTTF} \frac{\phi(0)}{kT}(1-2Kt)dt,$$

and

$$\frac{1}{2\langle \tau_{SD} \rangle} \approx \frac{\phi(0)}{kT}\left(K - \frac{1}{MTTF}\right).$$

This gives rise to

$$\frac{1}{MTTF} = K - \frac{kT}{2\phi(0)\langle \tau_{SD} \rangle} \approx K_0 e^{-\frac{E_k}{kT}}. \quad (15)$$

Eq. (15) is exactly the Prokopowicz-Vaskas equation where applied voltage is a constant![35] The degradation rate constant *K* can now be simply determined by an Arrhenius plot using the MTTF data obtained at various temperatures and at a constant voltage.

Table III summarizes MTTF data at a given voltage and different temperatures for BME A and BME B. A corresponding Arrhenius plot according to Eq. (15) is shown in FIG. 4. The activation energy E_k and degradation rate constant *K* can also be calculated.

Table III. Calculated MTTF Data from a Weibull Plot of Measured TTF Data

Temperature K	MTTF (hours)
BME B at 72V (4.5 times the rated voltage)	
408	384.75
428	50.50
438	16.63
448	6.46
BME A at 250V (5.0 times the rated voltage)	
428	546.00
438	136.80
448	24.11

Table IV lists the activation energy E_k and constant *K* at several temperatures for two BME capacitors. The barrier height $\phi(t)$ at the time the first catastrophic failure occurred can be estimated using Eq. (11) and the obtained *K* values in Table IV. For BME B, a 55% reduction of $\phi(0)$ can be calculated at 6.3 hour and 165°C when the average leakage current level is ~60 μA

(FIG. 1). For BME A, a 70% reduction at 367 hours and 155°C is obtained when the average leakage current level is ~80 μA. These results clearly show that a smaller value of the degradation rate constant *K* results in a slower IR degradation and a larger value of MTTF for the automotive-grade BME MLCC BME A than for BME B.

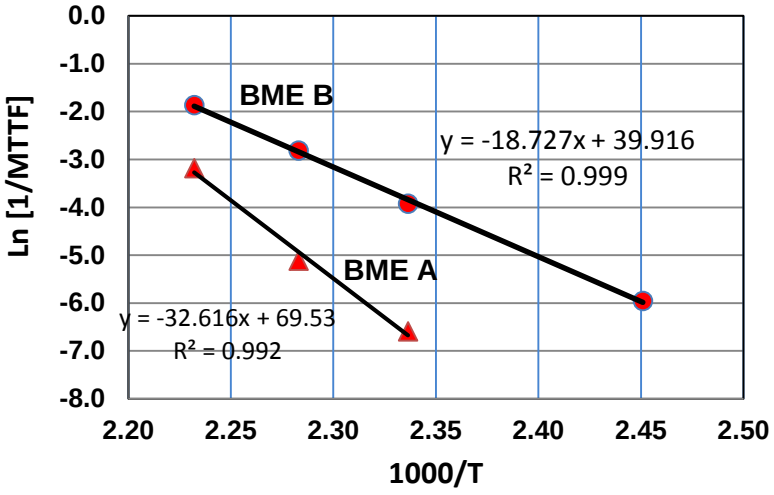

FIG. 4. Arrhenius plots using Eq. (15) and MTTF data in Table IV for BME capacitors BME A and BME B.

Table VI. Calculated Degradation Constant per the Curve-Fitting Results in FIG. 4

Part ID	$K_0 e^{\frac{-E_k}{kT}} (hour^{-1})$			
	E_k (eV)	at 398K (125°C)	at 428K (155°C)	at 438K (165°C)
BME A	2.590	8.865E-06	1.711E-03	8.423E-03
BME B	1.623	7.953E-04	2.152E-02	5.844E-02

D. IR degradation mechanism due to oxygen vacancy electromigration

According to Eq. (11), the barrier height degrades with an exponential relationship to stress time and can be expressed as

$$\phi(t) = \phi(0)\mathrm{e}^{-2\mathrm{Kt}},$$

where $K = K_0 e^{\frac{-E_k}{kT}}$ is the degradation rate constant. A slower degradation requires a smaller value of degradation constant *K* or a large value of E_k, which is the activation energy required for $V_O^{\bullet\bullet}$ to migrate and to be neutralized near the depletion layer at grain boundaries. Its value can be solely determined by the MTTF at a given stress level. The large value of E_k also means that the entrapment of $V_O^{\bullet\bullet}$ at grain boundaries may not be an energetically favorable process unless the

barrier height $\phi(t)$ is high enough to be comparable to E_k. This is the case for BME B, where a typical barrier height value of 1.30 eV has been reported.[4]

On the other hand, according to Eq. (14), a slower degradation, characterized by a larger value of $\langle\tau_{SD}\rangle$, would give rise to a smaller value of $\phi(0)$. This can be understood since a smaller $\phi(0)$ will promote the continuous electromigration of $V_O^{\bullet\bullet}$ without being trapped or localized at a grain boundary and cause an IR degradation (based on the degradation model proposed here, only those oxygen vacancies that have been trapped and neutralized will contribute to IR degradation). However, this is only one part of the equation: $\phi(0)$ also presents the barrier height for the conduction band electron carriers. A lower $\phi(0)$ will facilitate electron conduction and will deteriorate the IR as well. As a result, when electron conduction and oxygen vacancy electromigration are both taken into account, a moderate barrier height and a smaller *K* are the keys for minimal IR degradation in Ni-$BaTiO_3$-based MLCCs. As an important conclusion of this study, higher IR values may not always result in a larger MTTF, but a slower IR reduction rate (smaller *K*) always will. A higher $\phi(0)$ generally means higher resistance and therefore a higher electrical strength when a DC voltage is applied. This highly localized electric strength is more likely to cause the thermal-related electrical breakdown of the depletion layer and a reduction in the reliability life of the MLCCs.

According to Eq. (4), $N_d \gg n_s$, only a small fraction of oxygen vacancies will be trapped at the grain boundaries during the electromigration across the dielectric layer and will cause IR degradation. The majority of $V_O^{\bullet\bullet}$ will continually migrate and eventually reach the dielectric layer and internal Ni electrode interface, as has been revealed by previously reported electron energy loss spectroscopy (EELS) and high-resolution transmission electron microscope (HRTEM) observations.[4]

Since there is no evidence to show that $V_O^{\bullet\bullet}$ can be transferred across the cathode electrode layer, [4, 10] most $V_O^{\bullet\bullet}$ capable of migration will pile up along the Ni-electrode dielectric interface. To neutralize these vacancies, a significant amount of electrons is required, which can only be obtained from the cathode electron injection. The energy required for cathode electron injection must be much smaller than that of the Schottky barrier height at the dielectric-electrode interface (~1.25 eV[36]). The high concentration of localized electrons due to the compensation of the pile-

up of oxygen vacancies will not only dramatically change the local stoichiometry of $BaTiO_3$ dielectric, but it will also lead to a leakage current increase during IR degradation. This will cause a local temperature increase and will eventually lead to the breakdown at the Ni-$BaTiO_3$ interface. The initial failure site of the dielectric-electrode interface was revealed in a recently published failure analysis work on commercial BME MLCCs.[37]

IV. SUMMARY AND CONCLUSIONS

Two commercial BME capacitors with different quality levels were degraded under highly accelerated life test conditions to reveal the time-dependent IR degradation. The leakage current as a function of stress time was recorded in-situ for every capacitor sample tested. The leakage current data were found to fit well to an exponential relationship to the stress time and can be characterized by a characteristic growth time of τ_{SD}. τ_{SD} is the time at which the leakage current doubles its value and is therefore a measure of the degradation rate. The larger the value of τ_{SD}, the larger the MTTF.

The double Schottky barrier layer model at the ceramic grain boundary has been used to describe the resistivity of a BME capacitor. The barrier height $\phi(t)$ as a function of time has been found to follow

$$\phi(t) = \phi(0)\mathrm{e}^{-2\mathrm{Kt}},$$

where the degradation rate constant $K = K_0 e^{-\frac{E_k}{kT}}$ can be determined by the traditional Prokopowicz-Vaskas equation with respect to MTTF:

$$\frac{1}{MTTF} \approx K_0 e^{-\frac{E_k}{kT}}.$$

BME MLCCs with a larger MTTF should have a slower degradation rate and thus a smaller value of *K*.

On the other hand, the exponential growth time τ_{SD} determined during curve-fitting of the leakage current data has been found to relate to barrier height as

$$\frac{t - t_0}{\tau_{SD}} \approx -\frac{\phi(0)}{kT}\mathrm{e}^{-2\mathrm{Kt}},$$

indicating when temperature and time are constant, τ_{SD} is inverse to the grain boundary barrier height $\phi(0)$. This is due to the fact that a smaller $\phi(0)$ will promote the electromigration of $V_O^{\bullet\bullet}$, but there will be no entrapment at a grain boundary to cause an IR degradation. However, $\phi(0)$ is also the barrier for the conduction band electron carriers. A lower $\phi(0)$ will facilitate the electronic conduction and deteriorate IR as well. When electron conduction and oxygen vacancy migration are both taken into account, a moderate barrier height $\phi(0)$ and a small degradation rate constant $K_0 e^{-\frac{E_k}{kT}}$ are crucial for minimal IR degradation in Ni-$BaTiO_3$-based MLCCs.

In conclusion, higher IR values may not always result in an increased MTTF, but a slower rate of IR degradation, characterized by a smaller *K*, always will.

Acknowledgements

The author appreciates the NASA Electronic Parts and Packaging (NEPP) program's support for this study. The author also expresses his gratitude to Michael Sampson and Bruce Meinhold for reviewing the manuscript. The author would also like to thank the GSFC Code 562 Parts Analysis Laboratory for assistance with electrical testing.

References:

[1] H. Kishi, Y. Mizuno, and H. Chazono, Jpn. J. Appl. Phys., Part 1 **42**, 1 (2003).

[2] H. Chazono and H. Kishi, Jpn. J. Appl. Phys., Part 1 **40**, 5624 (2001).

[3] G. Y. Yang, G. D. Lian, E. C. Dickey, and C. A. Randall, D. E. Barber, P. Pinceloup, M. A. Henderson, R. A. Hill, J. J. Beeson, and D. J. Skamser, J. Appl. Phys., **96**, 7492 (2004).

[4] G. Y. Yang, G. D. Lian, E. C. Dickey, and C. A. Randall, D. E. Barber, P. Pinceloup, M. A. Henderson, R. A. Hill, J. J. Beeson, and D. J. Skamser, J. Appl. Phys., **96**, 7500 (2004).

[5] K. Morita, Y. Mizuno, H. Chazono, and H. Kishi, Jpn. J. Appl. Phys., Part 1 **41**, 6957 (2002).

[6] H. Chazono and H. Kishi, Key Eng. Mater. **248**, 183 (2003).

[7] D. F. K. Hennings, J. Eur. Ceram. Soc. **21**, 1637 (2001).

[8] K. Albertsen, D. Hennings, and O. Steigelmann, J. Electroceram. **2**, 193(1998).

[9] R. Waser, J. Am. Ceram. Soc. **72**, 2234 (1989).

[10] R. Waser, T. Baiatu, and K. H. Härdtl, J. Am. Ceram. Soc. **73**, 1645 (1990).

[11] R. Waser, T. Baiatu, and K. H. Härdtl, J. Am. Ceram. Soc. **73**, 1654 (1990).

[12] T. Baiatu, R. Waser, and K. H. Härdtl, J. Am. Ceram. Soc. **73**, 1663 (1990).

[13] W. Heywang, J. Am. Ceram. Soc., **47**, 484 (1964).

[14] G. Jonker, Solid State Electron. **7**, 895 (1964).

[15] G. Jonker, Mat. Res. Bull., **2**, 401 (1967).

[16] M. Vollman and R. Waser, J. Am. Ceram. Soc. **77**, 235 (1994).

[17] H. Kishi, Y. Mizuno, and H. Chazono, Jpn. J. Appl. Phys., Part 1 **42**, 1 (2003).

[18] T. Oyama, N. Wada, H. Takagi, and M. Yoshida, Phys. Rev. B **82**, 134107 (2010).

[19] W. Minford, IEEE Transactions on Components, Hybrids, and manufacturing Tech., **5**, 297 (1982).

[20] H. Pak, and B. Rawal, Proc. SPIE **3235**, 362 (1997).

[21] M. Randall, A. Gurav, D. Skamser, and J. Beeson, CARTS Proceedings, Scottsdale, AZ, 134 (2003).

[22] J. Yoon, K. Lee, and S. Lee, Tran. On Electrical and Electronic Mater. **10**, 1229 (2009).

[23] M. Cozzolino, CARTS Proceedings, Orlando, FL, 385, (2006).

[24] T. Ashburn and D. Skamser, Proceedings of the 5th SMTA Medical Electronics Symposium, 124 (2008).

[25] J. Paulsen and E. Reed, Microelectronics Reliability **42**, 815 (2002)

[26] D. Liu and M. Sampson, CARTS Proceedings, Jacksonville, FL, 45 (2011).

[27] D. Liu and M. Sampson, CARTS Proceedings, Las Vegas, NV, 59 (2012).

[28] D. Liu, CARTS Proceedings, Houston, TX, 235 (2013).

[29] D. Viehland, S. Jang and L. E. Cross, M. Wuttig, Phys. Rev. B **46**, 8003 (1992).

[30] T. Oyama, N. Wada, and H. Takagi, and M. Yoshiya, Physical Review B **82**, 134107 (2010).

[31] F. Kröger and H. J. Vink, *in Solid State Physics*, 307, (Academic Press, New York, 1956).

[32] K. Connors, *Chemical Kinetics, the study of reaction rates in solution*, (VCH Publishers, New York, 1991).

[33] T. Nakamura, T. Yao, J. Ikeda, N. Kubodera, and H. Takagi, IOP Conf. Series: Materials Science and Engineering **18**, 2007 (2011).

[34] E. Brzozowski and M. Castro, Journal of the European Ceramic Society **24**, 2499 (2004).

[35] T. I. Prokopowicz and A. R. Vaskas, Final Report ECOM-90705-F, NTIS AD-864068, (Oct. 1969).

[36] A. Polotai, I. Fujii, D. Shay, G. Yang, E. Dickey, and C. Randall, J. Am. Ceram. Soc., **91**, 2540 (2008).

[37] R. Weachock and D. Liu, CARTS Proceedings, Houston, TX, 165, (2013).

[38] J. Illingsworth, H. AI-Allak, and A. Brinkman, J. Phys. D: Appl. Phys. **23**, 971 (1990).